Characterisation of electron beam welded aluminium alloys

Article *in* Science and Technology of Welding & Joining · October 1999

DOI: 10.1179/136217199101537941

6 authors, including:

Gürel Çam
Iskenderun Technical University
19 PUBLICATIONS **188** CITATIONS
SEE PROFILE

V. Ventzke
Helmholtz-Zentrum Geesthacht
53 PUBLICATIONS **567** CITATIONS
SEE PROFILE

Jorge F. dos Santos
Helmholtz-Zentrum Geesthacht
335 PUBLICATIONS **5,415** CITATIONS
SEE PROFILE

M. Koçak
Gedik Holding, Gedik University
186 PUBLICATIONS **2,965** CITATIONS
SEE PROFILE

Characterisation of electron beam welded aluminium alloys

G. Çam, V. Ventzke, J. F. Dos Santos, M. Koçak, G. Jennequin, and P. Gonthier-Maurin

Electron beam (EB) welding was performed on three different aluminium alloys, namely alloys 2024, 5005, and 6061 (plate thickness 5 mm except alloy 5005 which was 3 mm in thickness), to establish the local microstructure–property relationships that would satisfy the service requirements for an electron beam welded aluminium alloy component with weld zone strength undermatching. Microstructural characterisation of the weld metals was carried out by optical and scanning electron microscopy. A very low level of porosity was observed in all EB welds owing to surface cleaning before welding and the vacuum environment of the EB welding process. Extensive microhardness measurements were also conducted in the weld regions of the joints. Global tensile properties and fracture toughness properties (in terms of crack tip opening displacement, CTOD) of the EB joints were determined at room temperature. The effects of strength mismatch and local microstructure on fracture toughness of the EB joints are discussed. The purpose of the present paper is to report the partial results of the European Brite–Euram project ASPOW (assessment of quality of power beam weld joints; BRPR–CT95–0021), which has been undertaken predominantly by industrial companies to establish a European framework for destructive and non-destructive testing and assessment criteria for laser and electron beam welds of over 20 metallic materials.

Dr Çam, Mr Ventzke, Dr Dos Santos, and Dr Koçak are at the GKSS Research Center, Institute of Materials Research, Max-Planck-Strasse, D–21502 Geesthacht, Germany, and Mr Jennequin and Mr Gonthier-Maurin are with CNIM, Zone Industrielle de Bregaillon, BP 208, F–83507 La Seyne-Sur-Mer Cedex, France. *Manuscript received 26 October 1998; accepted 4 February 1999.*

INTRODUCTION

The joining of aluminium alloys presents some difficulties, such as removal of the stable oxide layer from the surfaces in diffusion bonding and porosity formation as well as the occurrence of hot cracking and grain boundary liquation in fusion welding, i.e. arc welding and laser beam welding,[1–6] and therefore requires some special measures. Proper plate surface and edge cleaning, adequate use of filler wire, and weld pool shielding are normally used in the welding of aluminium alloys to ensure the production of welds free from gas porosity. Diamond machining just before welding was found to minimise pores in the weld metal of aluminium alloy 5083 joined by electron beam welding.[7]

In the present work, solid solution strengthened alloy 5005 and precipitation hardened aluminium alloys, namely 2024 and 6061, were butt welded by autogenous electron beam (EB) welding. The fusion welding of alloy 5005 is not expected to present any major difficulty. The formation of porosity may be the only concern in the welding of this alloy. On the other hand, the base metal mechanical properties may be degraded in autogenous welding of alloys 2024 and 6061. Furthermore, alloys 2024 and 6061 are both crack sensitive alloys, and thus are more difficult to fusion weld.[1–4] However, the high thermal gradient from the weld into the base metal in the low heat input EB process creates very limited metallurgical modifications, and crack sensitivity is therefore reduced. Owing to the low heat input, the heat affected zone (HAZ) produced in EB welding is very narrow,[5] and thus the problems associated with the HAZ are limited. However, as a result of the very high temperatures experienced in the fusion zone, the loss of some elements, for example vaporisation of magnesium, occurs during EB welding. The loss of such strengthening elements may degrade the mechanical properties of the welds by affecting the weld pool chemistry;[6,8] also, in this case the strength of the fusion zone cannot be restored to that of the base metal by post-weld heat treatment. Several researchers[6,8–15] have reported the loss of alloying elements in the welding of aluminium alloys. A common way of partially restoring the mechanical properties of the weld region is by the use of adequate filler alloy during welding.

The loss of strength in the fusion zone will cause a strain concentration in addition to the geometrical strain concentration that occurs if such a weld is exposed to an external loading. Confined plasticity development within the undermatched EB weld zone will therefore reduce the plastic straining capacity of the weld joint under tensile loading, as well as increasing the constraint within the weld zone.[16] An increase in constraint owing to confined plasticity may cause a reduction in the fracture toughness of the sandwiched fusion zone, compared to an 'all fusion zone' compact tensile (CT) specimen. Of course, such an 'all fusion zone' CT specimen is not realistic. There is a need to conduct an investigation to determine the level of fracture toughness and the effect of notch position (base metal, fusion zone, or HAZ) on fracture behaviour in strength undermatched EB weld zones of aluminium alloys.

In the present paper, the results of microstructural characterisation and mechanical testing of EB welded aluminium alloys, conducted to establish the local microstructure–property relationships of these joints, are discussed. Furthermore, the influence of the degree of strength loss (undermatching) in the fusion zone, including the HAZ, and the local microstructures on the fracture behaviour of the joints is determined.

EXPERIMENTAL PROCEDURE

Three different aluminium plates were studied in the present work: of alloys 5005-H14 (strain hardened only), 2024-T351 (solution heat treated, cold worked, naturally aged, and stretched), and 6061-T6 (solution heat treated and artificially aged). Plate thickness was 5 mm, except for alloy

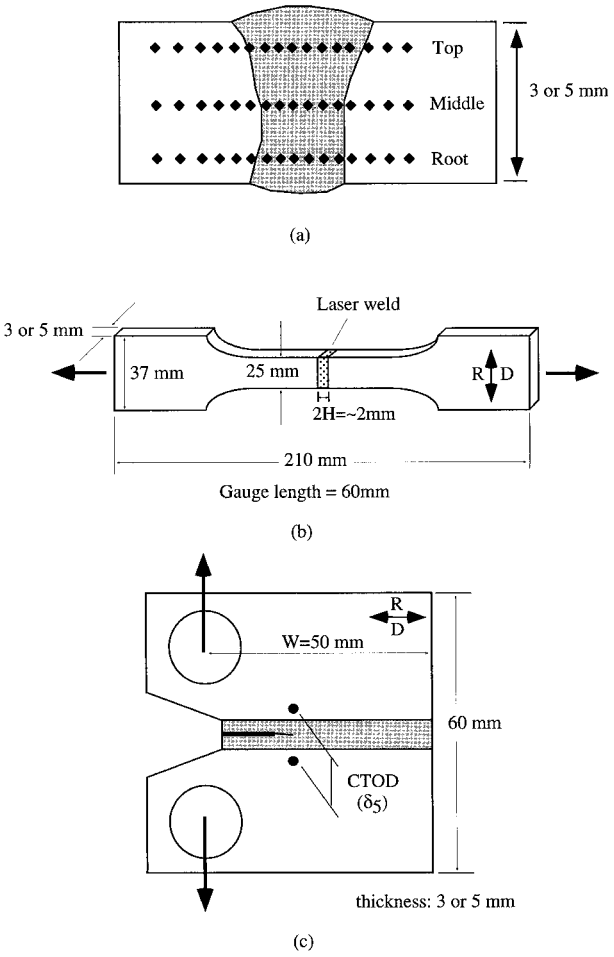

a hardness measurements; *b* tensile test specimen; *c* compact tension (CT) specimen with local crack tip opening displacement (CTOD) measurement technique of δ_5

1 Schematic diagrams of specimens for given tests

5005 which was 3 mm in thickness. The plate surfaces and weld edges were mechanically and chemically etched before welding, and butt welded parallel to the rolling direction by autogenous EB welding with travel speeds of 1·3, 1·4, and 1·5 m min^{-1}, respectively (Table 1). An accelerating voltage of 50 kV was used, except for welding alloy 5005 where the voltage was 30 kV. The beam currents used were 90, 130, and 120 mA, respectively.

Extensive optical and scanning electron microscopy including EDX analysis were conducted to investigate the microstructural changes taking place in the HAZ and fusion zone of the joints. For optical microscopy, all welds were etched with Kroll's reagent for 20 s. Microhardness measurements were conducted across the joints in three locations (i.e. top, mid, and root) to determine hardness profiles and variations in hardness along the weld depth (Fig. 1*a*).

Transverse tensile specimens, extracted from the baseplates perpendicular to the rolling direction, were tested to determine the mechanical properties of the base metals. The mechanical properties of the joints were determined by testing conventional flat transverse tensile specimens at room temperature (Fig. 1*b*). Standard compact tension (CT50) specimens were also extracted from the baseplates and the joints, and machine notched and fatigue precracked to introduce a sharp crack ($a/W = 0{\cdot}5$, where a is uncracked ligament, Fig. 1*c*). Room temperature fracture toughness tests were carried out on these specimens (about eight specimens for each notch position) as well as on base material specimens, to determine the R curves via the multiple specimen method. Welded specimens were tested at room temperature in the as welded condition without any further machining of the weld profile. Crack tip opening displacement (CTOD, δ_5) values were measured directly as shown in Fig. 1*c* using a δ_5 clip on gauge at the tip of the fatigue precrack, as described by Schwalbe *et al.*[17]

Table 1 Electron beam (EB) welding process parameters

Alloy	Plate thickness, mm	Welding speed, m min^{-1}	Accelerating voltage, kV	Beam current, mA
5005-H14	3	1·3	30	90
2024-T351	5	1·4	50	130
6061-T6	5	1·5	50	120

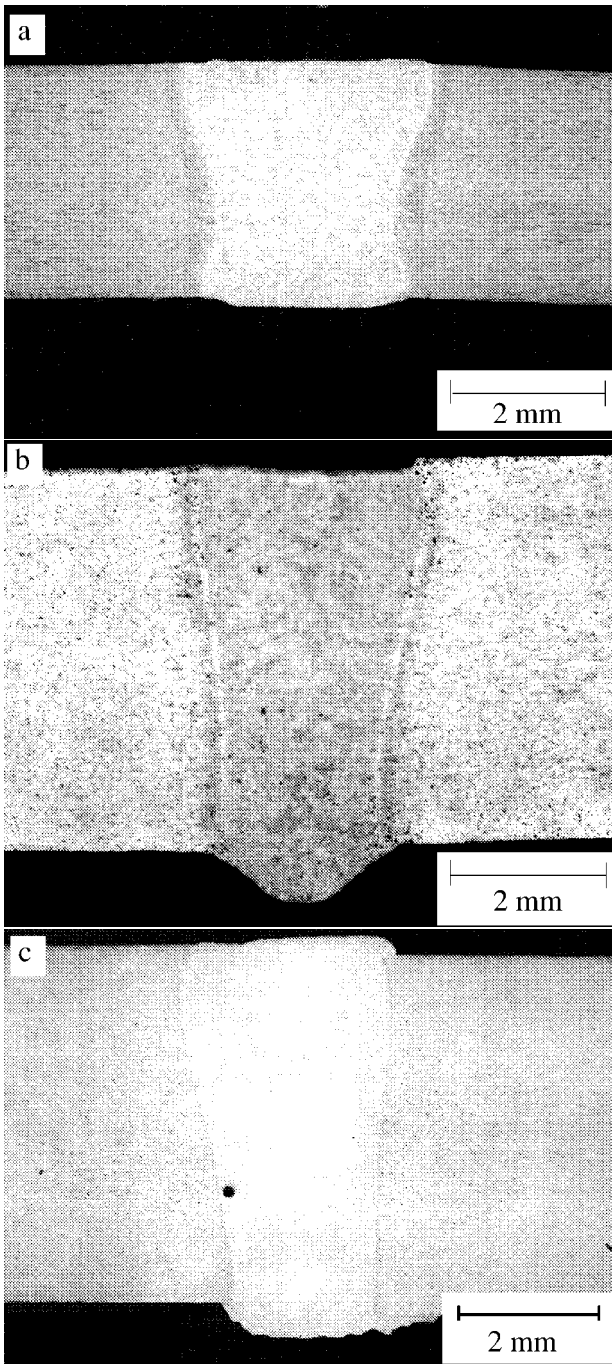

a 5005; *b* 2024; *c* 6061

2 Macrographs of electron beam (EB) welded joints

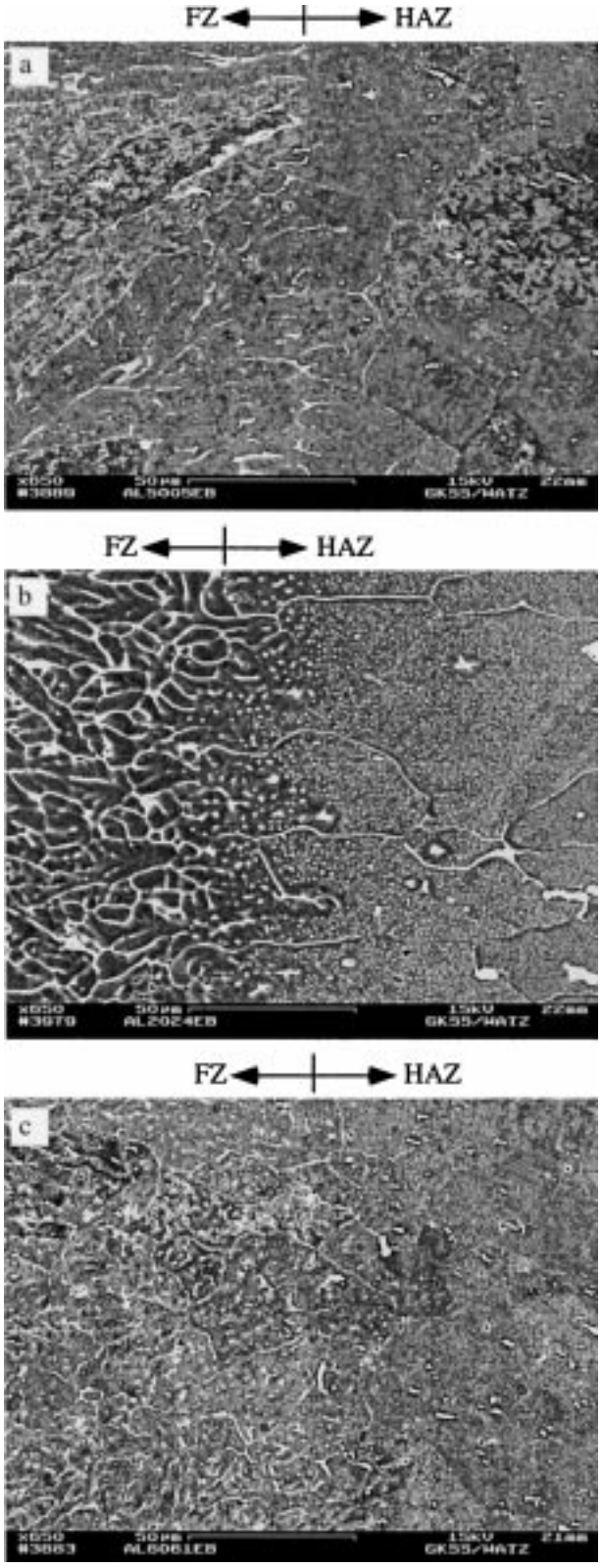

a 5005; *b* 2024; *c* 6061

3 Micrographs (SEM) showing heat affected zones (HAZs) of EB welded joints

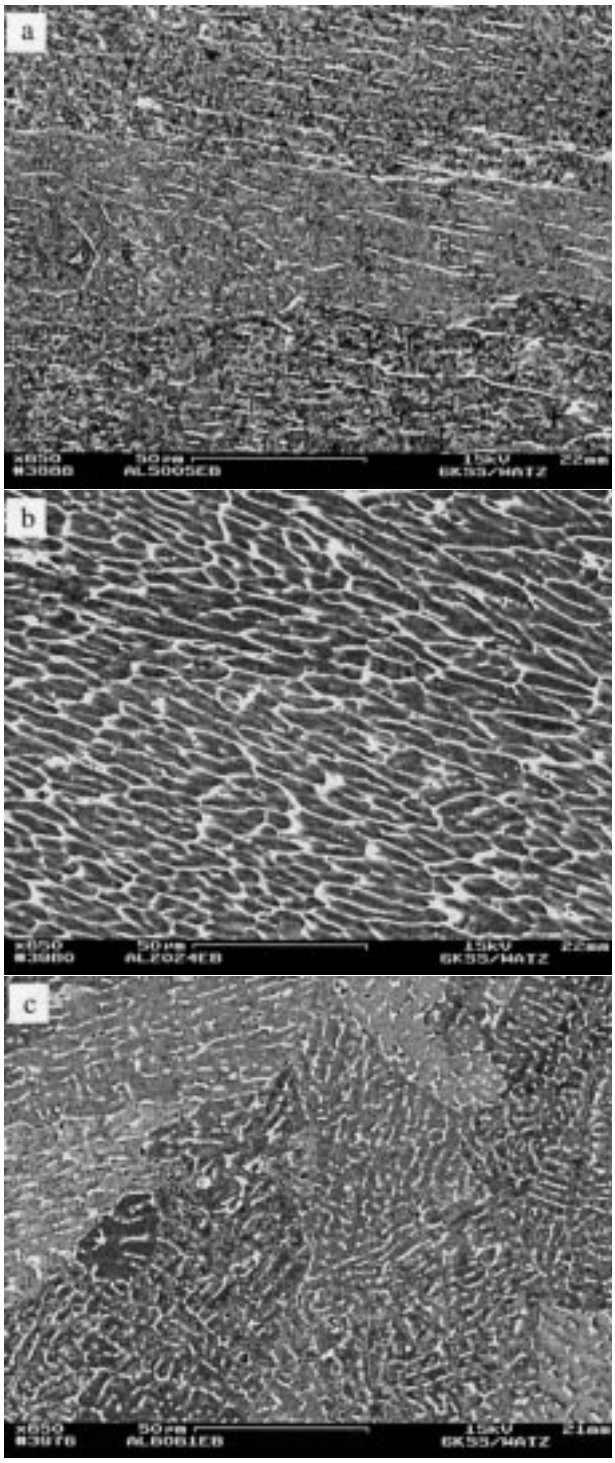

a 5005; *b* 2024; *c* 6061

4 Micrographs (SEM) showing fusion zones of EB welded joints

RESULTS AND DISCUSSION

Microstructural aspects of EB welds

Figure 2*a* shows a macrograph of an alloy 5005 EB welded joint, in which a narrow HAZ can be seen. However, the scanning electron micrograph of this joint does not reveal a distinct change in microstructure in the HAZ (Fig. 3*a*). The base material microstructure consisted of α-Al grains containing some iron rich particles, visible as a white phase in Fig. 3*a*. Results of SEM–EDX analysis indicated that these particles contained mainly iron and silicon. The actual stoichiometry of the phase was difficult to determine by EDX analysis. However, the concentrations of iron and silicon suggest that this phase is likely to be $Al_{15}Fe_3Si$ (Table 2). The fusion zone exhibited a fine grained microstructure with discontinuous iron rich precipitates containing some magnesium and silicon along the interdendritic regions, possibly α-Al and $Al_{15}Fe_3Si$, as well as fine iron rich particles within the grains (Table 2), visible

as a white phase in Fig. 4*a*. In addition to EDX point analyses, EDX area analyses (sampling an area large enough to take into account magnesium distribution) were conducted in the base material and fusion zone to determine the loss of alloying elements in the weld pool. The magnesium content of the fusion zone was ~0·4 wt-% lower than that of the base material, indicating that magnesium evaporation took place from the weld pool during EB welding of this alloy (Table 3). However, this alloy is a solid solution strengthened alloy (magnesium is a solid solution strengthener) and no loss of effective strengthening phases (fine precipitates) was involved; thus, this slight reduction in magnesium content (consequent loss of solid solution strengthening) is not very significant in reducing the strength level in the fusion zone.

A macrograph of an alloy 2024 EB welded joint is shown in Fig. 2*b*. The base material microstructure consisted of grains elongated in the rolling direction containing copper rich precipitates with some magnesium and silicon (Table 2), possibly Al_2Cu (θ phase) (Fig. 3*b*). Some large particles rich in iron, copper, and manganese were also observed in the base material. A narrow overaged HAZ region adjacent to the fusion zone containing coarsened Al_2Cu precipitates (Table 2) was observed (Fig. 3*b*). Some grain boundary liquation within the narrow HAZ was also observed. The fusion zone exhibited a structure with elongated dendritic networks decorated with copper rich precipitates, Al_2Cu, along the interdendritic boundaries owing to copper segregation, visible as a white phase in Fig. 4*b*. Magnesium evaporation from the weld pool of this joint also took place. Results of EDX area analysis indicated that the magnesium content of the base material was 2·7 wt-% whereas that of the fusion zone was ~2 wt-% (Table 3). It was also observed that the matrix phases of the fusion zone and HAZ contained less copper, i.e. 1·1 and 2·3 wt-%, respectively, than that of the base material, i.e. 3·6 wt-%. However, copper was depleted in the matrixes of these areas owing to the formation of extensive Al_2Cu precipitates (redistribution of copper in the fusion zone). Results of EDX area analysis (Table 3) showed that copper was 0·1% less in the fusion zone than in the base material, which is not significant in EDX terms, and indicated no vaporisation of copper during welding, taking into consideration the extent of copper rich precipitates.

A macrograph of an alloy 6061 EB welded joint is shown in Fig. 2*c*. The base material microstructure consisted of α-Al grains containing iron rich precipitates with some silicon (Table 2), possibly $Al_{15}Fe_3Si$ (Fig. 3*c*). No distinct HAZ was observed by optical and scanning electron microscopy (Fig. 3*c*). The fusion zone exhibited a fine grained dendritic microstructure with isolated (discontinuous) iron and silicon rich precipitates at the grain boundaries, possibly $Al_9Fe_2Si_2$ (Table 2), as well as within the grains, visible as a white phase in Fig. 4*c*, indicating iron and silicon segregation in the fusion zone. Results of EDX area analysis showed that the magnesium content was 0·3 wt-% less in the fusion zone than in the base material, which is not very significant in EDX terms (Table 3). However, the results suggest that some magnesium evaporation possibly took place during welding. The loss of magnesium from the weld pool during laser or EB welding of aluminium alloys has been reported by several researchers.[6,8–15] Area analysis by EDX also demonstrated that there was no silicon loss in the fusion zone as expected (Table 3).

Hardness of EB welds

The EB welded joint of alloy 5005 exhibited a hardness decrease of ~10–20% (strength undermatching) in the weld region, the hardness minimum lying in the HAZ region (Fig. 5*a*). The hardness reduction in the HAZ is apparently associated with the change in microstructure caused by the thermal cycle experienced during welding. Further investigations (TEM) are currently in progress to explain this situation. The reduction of hardness in the fusion zone is probably because of the loss of magnesium (solid solution strengthener) and/or microstructural changes.

In contrast to the alloy 5005 joint, the EB welded joint of alloy 2024 exhibited a significant hardness decrease in the fusion zone (high strength undermatching), but no appreciable hardness change in the HAZ (Fig. 5*b*). The

Table 2 Chemical compositions of particles observed in different regions of aluminium alloy weldments: values given are average of at least three readings, wt-% (at.-%)

Alloy	Region*	Al	Cu	Mg	Si	Mn	Fe	Cr
5005	BM	64·6 (78·1)	6·6 (3·4)	0·8 (1·1)	1·8 (2·1)	…	26·2 (15·3)	…
	FZ	86·6 (91·2)	…	2·2 (2·6)	1·0 (1·0)	…	10·2 (5·2)	…
2024	BM	51·9 (68·7)	43·1 (24·2)	4·1 (6·0)	0·9 (1·1)	…	…	…
	HAZ†	64·6 (77·9)	30·5 (15·6)	4·1 (5·5)	0·9 (1·0)	…	…	…
	FZ	64·4 (79·1)	32·7 (17·1)	2·4 (3·2)	0·5 (0·6)	…	…	…
6061	BM	61·8 (73·4)	1·4 (0·7)	0·5 (0·6)	7·7 (8·8)	…	25·8 (14·8)	2·1 (1·3)
	FZ	79·9 (85·9)	1·1 (0·5)	2·1 (2·5)	4·3 (4·5)	…	12·1 (6·3)	0·5 (0·3)

* BM is base material, FZ is fusion zone, HAZ is heat affected zone.
† Coarsened particles in HAZ.

Table 3 Area analysis results* (EDX) for EB welded aluminium alloys, wt-% (at.-%)

Alloy	Sampled region†	Al	Cu	Mg	Si	Mn	Fe	Cr
5005	BM	96·7 (96·5)	…	2·5 (2·7)‡	0·7 (0·7)‡	…	0·2 (0·1)	…
	FZ	97·0 (96·9)	…	2·1 (2·3)‡	0·6 (0·6)‡	…	0·3 (0·1)	…
2024	BM	92·2 (94·5)	4·2 (1·8)‡	2·7 (3·1)‡	0·4 (0·4)‡	0·5 (0·2)	…	…
	FZ	93·1 (95·4)	4·1 (1·7)‡	2·0 (2·3)‡	0·4 (0·4)‡	0·5 (0·2)	…	…
6061	BM	96·0 (96·2)	…	2·5 (2·8)‡	0·7 (0·7)‡	0·1 (0·1)	0·5 (0·2)	0·2 (0·1)
	FZ	96·1 (96·3)	…	2·2 (2·5)‡	0·8 (0·8)‡	0·1 (0·1)	0·5 (0·3)	0·2 (0·1)

* Values are average of at least three readings.
† BM is base material, FZ is fusion zone.
‡ Change in concentration.

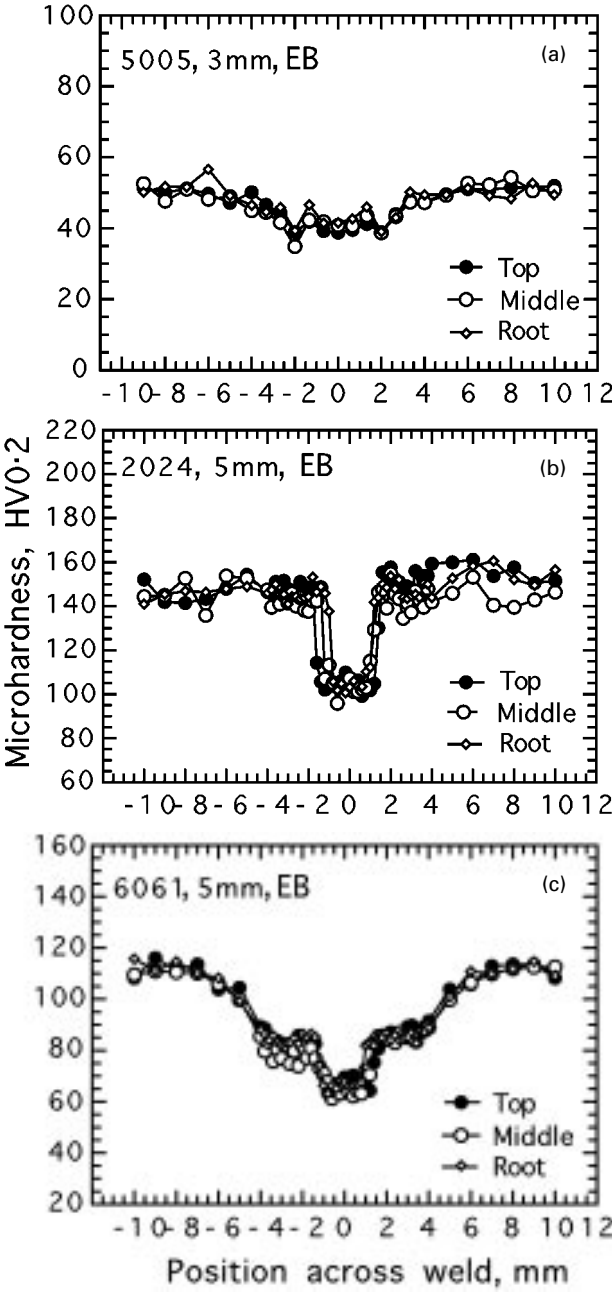

a 5005; *b* 2024; *c* 6061

5 Hardness profiles of EB welded joints: spacing and orientation between hardness indentations were varied in different regions of welds to obtain detailed information

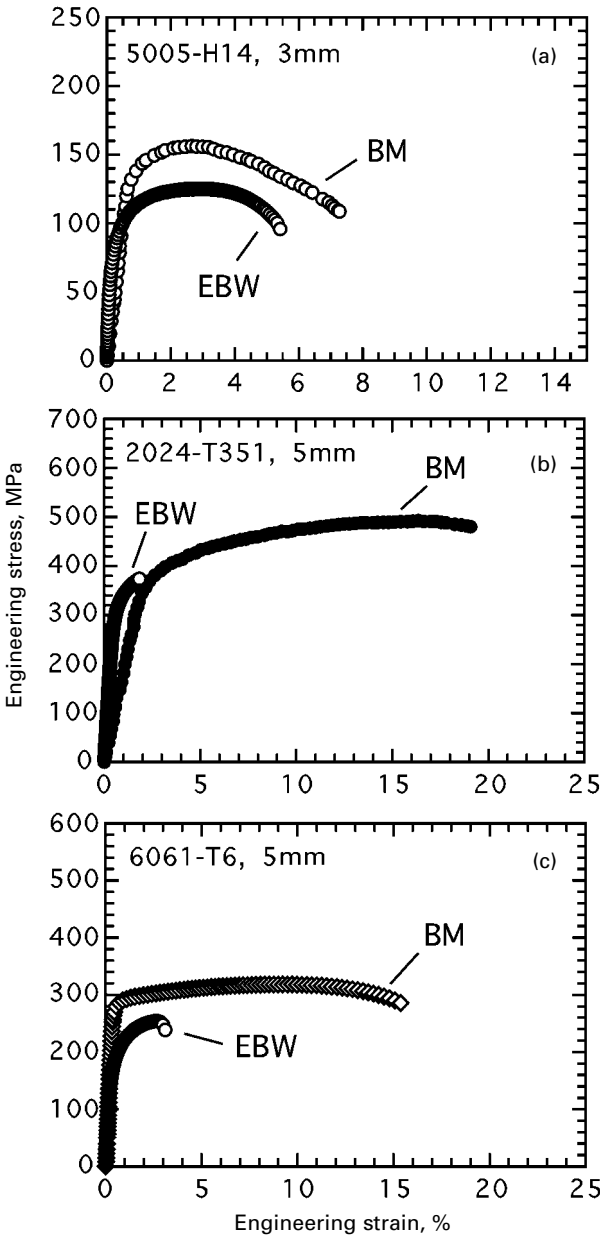

a 5005; *b* 2024; *c* 6061

6 Comparison of stress–strain curves of respective baseplates (BM) and transverse tensile specimens of EB welded (EBW) joints: note significant reduction in straining capacity of EB welds of 2024 and 6061 alloys owing to strength undermatching in fusion zone

reason for the hardness loss in the fusion zone is the loss of strengthening phases associated with copper.

The hardness minimum also lay in the fusion zone of the alloy 6061 EB welded joint (Fig. 5*c*), possibly as a result of microstructural changes taking place during welding, i.e. magnesium and silicon segregation into the inter-dendritic regions in the fusion zone and the consequent formation of non-strengthening Mg_2Si particles (presumably the coarsening of β'' phase to form β' particles). Therefore, the loss of hardness in the fusion zone seems to result from the coarsening of the strengthening phases (β'' phase, Mg_2Si). A hardness decrease was also present in the HAZ of this joint as well as in the fusion zone, which corresponds to the overaged HAZ region where the coarsening of non-strengthening β' precipitates (Mg_2Si) took place. However, the hardness of the HAZ was higher than that of the fusion zone, in contrast to conventional welds where the hardness minimum lies in the overaged HAZ region.[18] The reason for this seems to be the use of filler wire in arc welding, which increases the hardness in the fusion zone. The minimum hardness values in the present HAZ regions are remarkably similar to those in arc welding, supporting the above explanation.

Tensile properties

Global tensile properties of the autogenous EB welded joints were determined by testing conventional flat transverse tensile specimens, at room temperature, without machining the weld reinforcement. The results are summarised in Table 4, which also includes the base metal properties. All EB welded joints failed in the weld region owing to the strength undermatching condition (the strength loss in the fusion zone; *see* hardness profiles, Fig. 5).

The ductility of the alloy 5005 joint was similar to that of the base metal, i.e. 77% of that of the base metal (Fig. 6*a*), owing to the fact that the hardness loss in the weld region of this joint was insignificant (Fig. 5*a*). The joint efficiency in terms of tensile strength was ~79%. Transverse tensile test results showed significant losses of ductility in 2024 and 6061 alloys (Fig. 6*b* and *c*), owing to strain concentration in the lower strength fusion zone, as expected from the hardness profiles (Fig. 5*b* and *c*). The strength of aluminium alloys is derived from solid solution strengthening and/or precipitation hardening, and the loss of alloying elements (solid solution strengtheners or precipitate formers) leads to a decrease in strength of the fusion zone. The joint efficiencies in terms of tensile strength were found to be ~70% and 80% for alloys 2024 and 6061, respectively, whereas the joint efficiencies in terms of elongation were very low, ~6·3% and 19·2%, respectively, owing to the significant undermatching in the weld zones. In the case of undermatching, the stress concentration and, thus, fracture take place in the lower strength weld metal region of the joints (confined plasticity), leading to an increase of constraint within the weld region and, thus, significantly lower ductility levels.

It can be concluded that strength undermatched EB welds can provide rather high loading capacity in terms of strength (because of confined plasticity), but not in terms of strain under tensile loading conditions.

Fracture toughness

Fracture toughness tests (CTOD) were carried out on the base materials and EB welded joints at room temperature to determine the toughness values using CT50 specimens as shown in Fig. 1. The results of three fracture toughness tests conducted on the baseplates and the specimens extracted from the joints with different crack positions, i.e. fusion zone and HAZ cracked, are summarised in Table 5. These CTOD values δ_{5m} were obtained at the onset of maximum load levels. The specimens were unloaded after attainment of maximum load level and then refatigue cracked to measure the stable crack growth Δa.

As seen from Table 5, the base material specimens of alloys 5005 and 6061 exhibited the lowest fracture toughness value, i.e. CTOD $(\delta_{5m}) = 0{\cdot}29$ and 0·24 mm, respectively. Fusion zone cracked specimens displayed fracture toughness values of 1·19 and 0·57 mm, respectively, higher than those of the respective baseplates because of the strength undermatching nature of the fusion zones. The HAZ cracked specimens of alloy 5005 are currently being tested. For each weld zone, about eight specimens were tested to establish the *R* curve (the multiple specimen technique). The *R* curves of the base materials, fusion zones, and HAZs for alloys 5005, 2024, and 6061 are shown in Fig. 7. It is interesting to point out that, for the alloy 6061 EB welded joint, the fusion zone displayed the highest fracture toughness, followed by the HAZ, and the lowest fracture toughness was exhibited by the baseplate (Fig. 7*c*); this is expected from the hardness profile of this joint (Fig. 5*c*), which displayed a relatively wide overaged HAZ region, typical of this alloy, although optical and scanning electron microscopy failed to resolve this region.

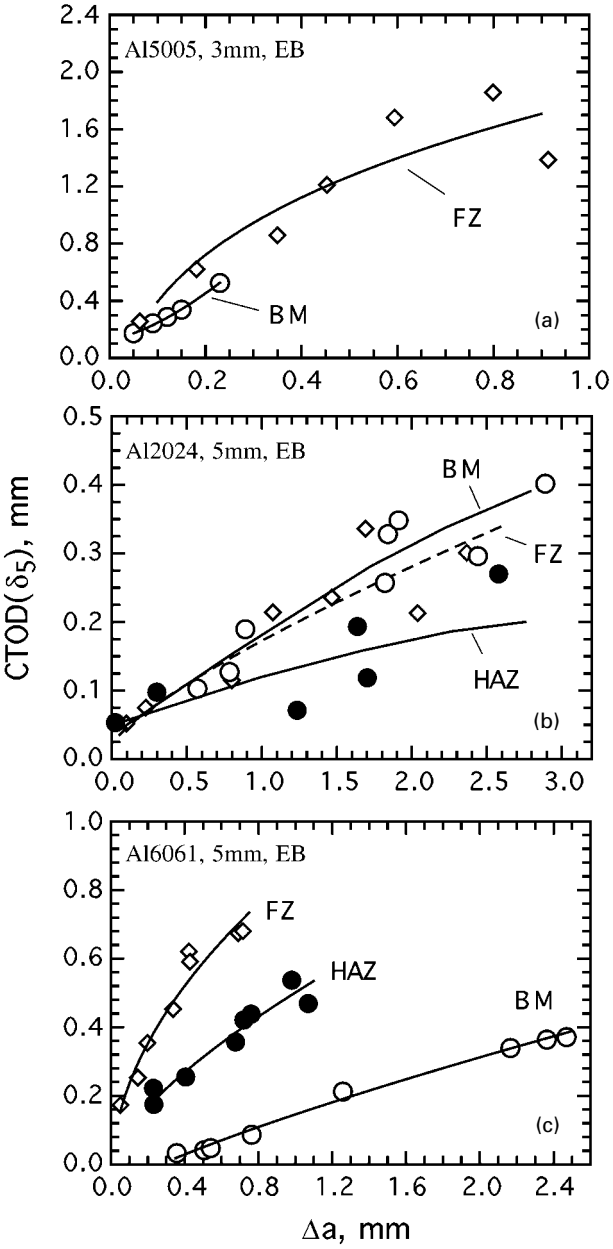

a 5005; *b* 2024; *c* 6061

7 Crack tip opening displacement (CTOD) *R* curves of baseplates (BM) and EB welded joints: FZ is fusion zone

In the case of the alloy 2024 EB welded joint, the fusion zone and HAZ specimens exhibited slightly lower fracture toughness values, i.e. CTOD $(\delta_{5m}) = 0{\cdot}17$ and 0·11 mm, respectively, than the baseplate specimens, i.e. CTOD

Table 4 Results of tensile tests: values given are average of those for three specimens

Material*	Yield strength $R_{p0{\cdot}2}$, MPa	Tensile strength R_m, MPa	Elongation A, %	Joint efficiency in terms of R_m, %	Joint efficiency in terms of A, %
5005 (BM)	147	158	7·0	...	...
5005 (EBW)	96	125	5·4	79·1	77·1
2024 (BM)	350	493	19·0	...	...
2024 (EBW)	312	348	1·2	70·6	6·3
6061 (BM)	281	319	15·6	...	...
6061 (EBW)	182	255	3·0	80·0	19·2

* BM is base material, EBW is electron beam weld.

Table 5 Fracture toughness values CTOD (δ_{5m}) of joints and respective base materials, mm

Alloy	Base material	Fusion zone	Heat affected zone
5005-H14	0·43	1·43	Tests in progress
	0·34	1·37	
	0·29*	1·19*	
2024-T351	0·31	0·20	0·14
	0·29	0·19	0·13
	0·29*	0·17*	0·11*
6061-T6	0·28	0·62	0·43
	0·31	0·60	0·42
	0·24*	0·57*	0·41*

* Minimum value for three specimens tested.

(δ_{5m}) = 0·29 mm, although the joint showed a strength undermatching in the weld region (*see* hardness profile, Fig. 5*b*). The reason for this unexpected low fracture toughness is apparently the formation of very distinct dendritic networks containing brittle precipitates (Al_2Cu) along the boundaries in the fusion zone, and the coarsening of brittle particles in the HAZ of this joint. As seen in Fig. 3*b*, the coarsened Al_2Cu particles and liquated grain boundaries in the overaged HAZ region and the continuous boundaries between elongated dendritic grains containing Al_2Cu particles presented a favourable crack path, leading to low fracture toughness, although the fusion zone exhibited a strength undermatching. Ductile crack growth during CTOD testing occurred predominantly along the boundary region (within the fusion zone) adjacent to the base metal, owing to the discontinuity of mechanical properties between the base material and fusion zone. Furthermore, intergranular fracture in the fusion zone of alloy 7020, occurring along the liquated grain boundaries, was observed and details can be found elsewhere.[19] Post-test sectioning and SEM work on fracture surfaces are currently in progress, to demonstrate intergranular fracture in the fusion zone of alloy 2024 in particular.

CONCLUSIONS

The following conclusions have been drawn from the present work.

1. Defect free welds in aluminium alloys 5005, 2024, and 6061 were produced by autogenous electron beam (EB) welding. However, a low level of porosity was still observed in most cases, which is considered to be acceptable for aluminium alloy weldments.

2. The results indicate magnesium loss in the fusion zone of all the joints during welding. No distinct heat affected zone (HAZ) in terms of microstructure was observed in the alloy 5005 joint, although a clear hardness minimum was seen in the HAZ region in the hardness profile. The hardness profile of the alloy 6061 joint indicated an overaged HAZ region. In the alloy 2024 joint, a narrow HAZ region with particle coarsening (overaged region) was also observed. The fusion zone of the alloy 2024 joint exhibited columnar dendritic grain formation decorated with particles, whereas the fusion zones of alloys 5005 and 6061 showed a dendritic solidification microstructure with isolated particles along the grain boundaries, as well as within the grains.

3. The EB welded joints exhibited minimum hardness in the fusion zones (strength undermatching), most likely resulting from loss of strengthening elements and/or phases (dissolution). Although the hardness minimum lay in the HAZ region of the alloy 5005 joint, the hardness reduction in the fusion zone was not as pronounced as those in the other two joints. The coarsening of strengthening phases is possibly responsible for the hardness reduction in the HAZ regions.

4. Transverse tensile test results of autogenous EB welded joints showed slight decreases in strength and significant losses in ductility for alloys 2024 and 6061, owing to strain concentration in the narrow, lower strength fusion zone (~2 mm in width), although the alloy 5005 joint exhibited a relatively high ductility level, compared to the respective baseplate.

5. The fusion zone of the alloy 5005 joint as well as the fusion zone and HAZ of the alloy 6061 joint exhibited significantly higher fracture toughness than that of the base material, and thus displayed higher resistance to stable crack growth. The fusion zone of the alloy 2024 joint exhibited similar or slightly lower fracture toughness values than those of the respective baseplate, whereas the HAZ region showed the lowest *R* curve behaviour.

ACKNOWLEDGEMENTS

This work is a part of the Brite–Euram ASPOW project (BRPR95–0021). The authors wish to thank the European Commission for financial support, and Ms M. Bialinska and Mr S. Riekehr for conducting the mechanical tests.

REFERENCES

1. S. KUO: *Weld. Res. Counc. Bull.*, 1986, (320).
2. G. ÇAM and M. KOÇAK: *Sci. Technol. Weld. Joining*, 1998, **3**, 159–175.
3. G. ÇAM and M. KOÇAK: *Int. Mater. Rev.*, 1998, **43**, 1–44.
4. G. ÇAM, J. F. DOS SANTOS, and M. KOÇAK: 'Laser and electron beam weldability of Al-alloys: literature review', GKSS Report 97/E/25, IIW Document IX–1896–98. GKSS Research Center, Geesthacht, 1997.
5. D. L. OLSEN *et al.* (ed.): 'ASM handbook: welding, brazing, and soldering', Vol. 6; 1993, Materials Park, OH, ASM International.
6. L. A. GUITTEREZ, G. NEYE, and E. ZSCHECH: *Weld. J.*, 1996, **75**, 115s–121s.
7. J. L. MURPHY, R. A. HUBER, and W. E. LEVER: *Weld. J.*, 1990, **69**, 125s–132s.
8. J. RAPP, C. GLUMANN, F. DAUSINGER, and H. HÜGEL: in 'The effect of magnesium evaporation in laser welding of aluminium alloys', 275–282; 1993, Paris, Institut de Soudure.
9. J. RAPP, M. BECK, F. DAUSINGER, and H. HÜGEL: in 'Fundamental approach to the laser weldability of aluminium- and copper-alloys', 313–325; 1994, Düsseldorf, DVS.
10. M. J. CIESLAK and P. W. FUERSCHBACH: *Metall. Trans. B*, 1998, **19B**, 319–329.
11. D. A. SCHAUER, W. H. GIEDT, and S. M. SHINTAKU: *Weld. J.*, 1978, **57**, 127s–133s.
12. A. BLOCK-BOLTEN and T. W. EAGER: *Metall. Trans. B*, 1984, **15B**, 461–469.
13. A. BLAKE and J. MAZUMDER: *J. Eng. Ind. (Trans. ASME)*, 1985, **107**, 275–280.
14. D. W. MOON and E. A. METZBOWER: *Weld. J.*, 1983, **62**, 53s–58s.
15. W. XIJING, S. KATAYAMA, and A. MATSUNAWA: *Weld. J.*, 1997, **76**, 70s–73s.
16. Y.-J. KIM: 'Strength mis-match effect on local stresses and its implication to structural assessments', Documents X–1415–98, SC X–F–081–98, IIW, Paris, 1998.
17. K.-H. SCHWALBE, B. K. NEALE, and J. HEERENS: 'The GKSS test procedure for determining the fracture behaviour of materials: EFAM GTP 94', Report 94/E/60, GKSS Research Center, Geesthacht, 1994.
18. L. A. GUITTEREZ, G. NEYE, and E. ZSCHECH: *Weld. J.*, 1996, **75**, 115s–121s.
19. G. ÇAM, V. VENTZKE, J. F. DOS SANTOS, M. KOÇAK, G. JENNEQUIN, and P. GONTHIER-MAURIN: unpublished report, 'Microstructural and mechanical characterization of electron beam welded Al-alloy 7020'.